

1 Substantial root-zone water storage capacity observed by GRACE 2 and GRACE/FO

3 Meng Zhao¹, Erica L. McCormick², Geruo A³, Alexandra G. Konings², Bailing Li^{4,5}

4 ¹Department of Earth and Spatial Sciences, University of Idaho, Moscow, ID 83843, U.S.

5 ²Department of Earth System Science, Stanford University, Stanford, CA 94305, U.S.

6 ³Department of Earth System Science, University of California, Irvine, CA 92617, U.S.

7 ⁴NASA Goddard Space Flight Center, Greenbelt, MD 20771, U.S.

8 ⁵Earth System Science Interdisciplinary Center, University of Maryland, College Park, MD 20742, U.S.

9

10 *Correspondence to:* Meng Zhao (mengz@uidaho.edu)

11 **Abstract.** Root-zone water storage capacity (S_r) - the maximum water volume available for vegetation uptake - bolsters
12 ecosystem resilience to droughts and heat waves, influences land-atmosphere exchange, and controls runoff and groundwater
13 recharge. In land models, S_r serves as a critical parameter to simulate water availability for vegetation and its impact on
14 processes like transpiration and soil moisture dynamics. However, S_r is difficult to measure, especially at large spatial scales,
15 hindering an accurate understanding of many biophysical processes, such as photosynthesis, evapotranspiration, tree mortality,
16 and wildfire risk. Here, we present a global estimate of S_r using measurements of total water storage (TWS) anomalies from
17 the Gravity Recovery and Climate Experiment (GRACE) and GRACE Follow-On satellite missions. We find that the median
18 S_r value for global vegetated regions is at least 220 ± 40 mm, which is over 50% larger than the latest estimate derived from
19 tracking storage change via water fluxes, and 380% larger than that calculated using a typical soil and rooting depth
20 parameterization. These findings reveal that plant-available water stores exceed the storage capacity of 2-meter-deep soil in
21 nearly half of Earth's vegetated surface, representing a notably larger extent than previous estimates. Applying our S_r estimates
22 in a global hydrological model improves evapotranspiration simulations compared to other S_r estimates across much of the
23 globe, particularly during droughts, highlighting the robustness of our approach. Our study highlights the importance of
24 continued refinement and validation of S_r estimates and provides a new observational approach for further exploring the
25 impacts of S_r on water resource management and ecosystem sustainability.

26 1 Introduction

27 During periods of insufficient precipitation, vegetation relies on water stored underground to survive (Miguez-Macho
28 and Fan, 2021). The larger the root-zone water storage capacity (S_r), the more water the root zone can store during wet periods
29 for use in droughts (Teuling et al., 2006). S_r , therefore, plays an important role in regulating ecosystem resilience to droughts
30 and heat waves and affecting wildfire outbreaks and mortality risk (Callahan et al., 2022; Chen et al., 2013; Goulden and Bales,
31 2019; Hahm et al., 2019; Humphrey et al., 2018; Stocker et al., 2023). It is also an essential parameter for modelling plant

32 carbon uptake, transpiration, soil evaporation, streamflow, and groundwater (Maxwell and Condon, 2016; Zhao et al., 2022;
33 Peterson et al., 2021). Despite its critical role in modulating the carbon and water cycles, global patterns of S_r remain poorly
34 characterized.

35 The S_r is typically calculated as the integration of plant rooting depth and soil texture-dependent water-holding
36 capacity (Seneviratne et al., 2010; Vereecken et al., 2022; Speich et al., 2018; Federer et al., 2003). However, this approach
37 (hereafter referred to as the rooting depth-based estimation) suffers from uncertainties associated with plant rooting depth and
38 substrate hydraulic properties, particularly at depth, both of which undermine the accuracy of the calculated S_r (Vereecken et
39 al., 2022; Novick et al., 2022). Moreover, this approach assumes a static root zone confined to the near surface unsaturated
40 soil layer. However, recent studies have shown that this assumption is not always accurate. In many ecosystems, plant roots
41 can penetrate beyond the shallow soil layer into weathered bedrock, accessing rock moisture and tapping into groundwater,
42 especially during prolonged dry periods (Li et al., 2015; Hahm et al., 2020; McCormick et al., 2021; Rempe and Dietrich,
43 2018; Maxwell and Condon, 2016; Fan et al., 2017; Baldocchi et al., 2021). Thus, the rooting depth-based estimation may
44 significantly underestimate S_r .

45 More recently, Earth observations of precipitation (P) and evapotranspiration (ET) have been used to estimate S_r .
46 Several studies (Stocker et al., 2023; Wang-Erlandsson et al., 2016; Gao et al., 2014; McCormick et al., 2021) have proxied S_r
47 using the maximum cumulative difference in ET and P during dry periods (when $ET > P$), which reflects the largest water
48 volume that an ecosystem has withdrawn from its root zone. This method (hereafter referred to as the water deficit-based
49 estimation) is based on mass balance and thus eliminates the need for assumptions about plant access to rock moisture and
50 groundwater, rooting depth, and soil and bedrock hydraulics. However, obtaining accurate P and ET data is challenging at
51 scale (Sun et al., 2018; Miralles et al., 2016), and errors in these data can accumulate and deteriorate S_r calculations. Here, to
52 avoid this shortcoming, we estimated root-zone storage dynamics directly from total water storage (TWS) anomalies measured
53 by the Gravity Recovery and Climate Experiment (GRACE) and GRACE Follow-On (GRACE-FO) satellite missions
54 (hereafter GRACE/FO). With these observations, we characterized global patterns of S_r and found that both the rooting depth-
55 based estimate and the water deficit-based estimate have significantly underestimated S_r .

56 **2 Materials and methods**

57 **2.1 GRACE/FO TWS**

58 We use monthly measurements of the TWS anomaly from GRACE for the years 2002-2017 and from GRACE-FO
59 for the years 2018-2022. These measurements were obtained from the Jet Propulsion Laboratory (JPL) RL06 solutions
60 (Watkins et al., 2015; Wiese et al., 2016), which provide monthly average anomalies of the gravity field over an equal-area
61 $3^\circ \times 3^\circ$ mass concentration block (mascon). We opted for the JPL mascon solutions because each JPL mascon is relatively
62 uncorrelated with neighbouring mascons and thus offers more localized spatial variations than other mascon solutions and the
63 spherical harmonic solutions (Watkins et al., 2015; Wiese et al., 2016). We did not fill the 11-month gap (July 2017 to May

2018) between GRACE and GRACE-FO. However, we linearly interpolated other missing months from the nearest previous and subsequent non-missing values (Rodell et al., 2018; Zhao et al., 2021). Because we aimed to estimate root-zone storage capacity S_r , we only included mascon locations with over 50% fractional vegetation cover based on the land cover product (MCD12Q1) version 6.1 from the Moderate Resolution Imaging Spectroradiometer (MODIS) (Sulla-Menashe and Friedl, 2018).

2.2 S_r from TWS drawdown and uncertainty estimate

Ecosystem use of land water storage for ET is reflected in TWS drawdowns, consecutive declines in TWS despite seasonal or intermittent recharge and after accounting for long term trend due to anthropogenic groundwater use. An example is illustrated in Fig. 1 at a mascon location in southern Idaho, where the largest TWS drawdowns are annotated. From the water balance, a TWS drawdown over a time-period Δt is equal to:

$$\Delta TWS = \sum P - \sum ET - \sum R \quad (1)$$

where $\sum P$, $\sum ET$, and $\sum R$ are the total precipitation, total evapotranspiration, and net runoff out of the mascon over Δt , respectively. Based on eq (1), when precipitation exceeds runoff ($\sum P - \sum R > 0$), any TWS drawdown (or negative ΔTWS) must be influenced by a change in storage due to ET. To determine if precipitation exceeds runoff during GRACE/FO-observed TWS drawdowns, we compared R estimates from a multi-forcing observation-based global runoff reanalysis (Ghiggi et al., 2021) to P estimates from the Global Precipitation Climatology Project (Gebremichael et al., 2003). We found that in nearly all analysed mascon locations, the average $P - R$ is positive during at least the five largest TWS drawdowns (Fig. A1), confirming these TWS drawdowns reflect root-zone water storage transpired by ecosystems and not loss of water in the mascon due to runoff.

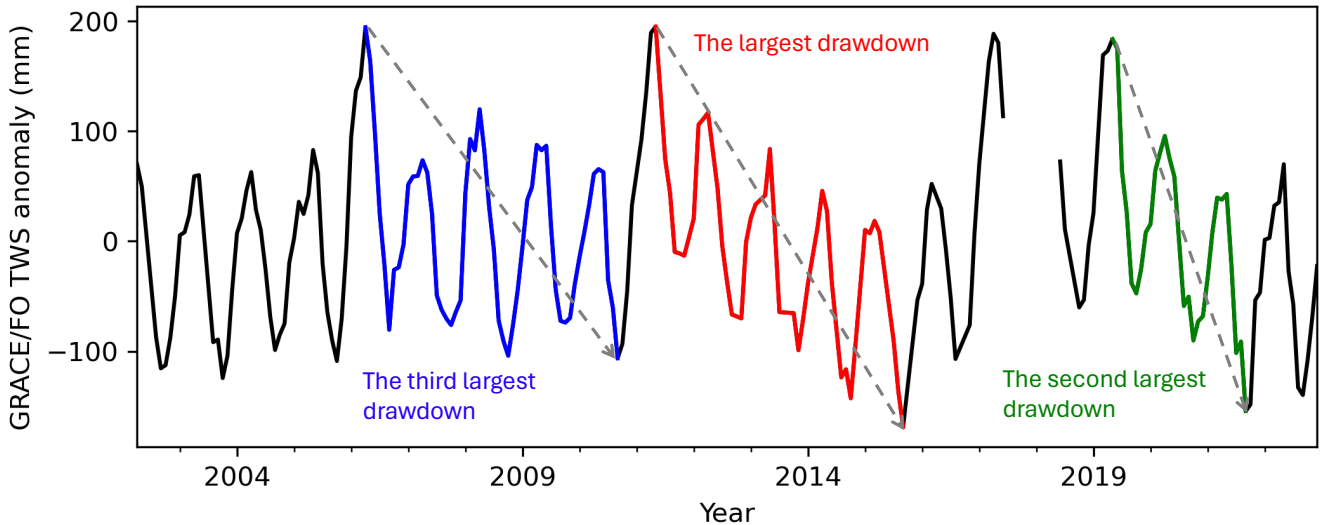


Figure 1. TWS time series showing the three largest drawdowns at a mascon location in southern Idaho.

84

85

86

87

88

89

90

91

92

93

94

95

96

97

98

99

100

101

102

103

104

105

106

107

108

109

110

111

112

113

114

115

We estimated root-zone water storage capacity S_r to be the largest TWS drawdown during the record period of GRACE/FO (denoted as $S_r^{GRACE/FO}$). To avoid overestimating S_r , we removed the impact of groundwater pumping, snow, and surface water on TWS drawdowns. Anthropogenic groundwater use often manifests as a negative long-term trend in the TWS time series (Rodell et al., 2018; Rodell et al., 2009; Feng et al., 2013). For example, regions showing significant TWS decreasing trends largely coincide with well-known groundwater irrigation areas identified in AQUASTAT data (Fig. A2). To avoid conflating this drawdown with S_r , we first calculated the TWS trend by simultaneously fitting an annual and a semi-annual signal, a linear trend, and a constant to the GRACE/FO time series (Fig. A2). Then, we assumed any negative trend was attributable to groundwater pumping and removed the negative trend from the original GRACE/FO time series before calculating the TWS drawdowns. In high-latitude and mountainous regions, the maximum TWS anomaly during drawdowns may include snow. To avoid attributing snow storage to root-zone water storage, we first determined the largest drawdown from the full GRACE/FO time series and then calculated S_r using the maximum and minimum TWS anomaly with a monthly mean air temperature above 5°C. We obtained air temperature data from the fifth-generation European Centre for Medium-Range Weather Forecasts atmospheric reanalysis of the global climate (ERA5) (Hersbach et al., 2020). Following Wang et al. (2023a), we used total runoff from Ghiggi et al. (2021), which includes both surface runoff and subsurface runoff, as a proxy for surface water storage change (i.e., $\Delta SW = R$) and removed it from TWS drawdowns to isolate ΔSW contributions (water stored in rivers, lakes, and reservoirs) to the GRACE/FO signal. This approach assumes that (1) R directly contributes to an increase in surface water levels within the drainage network, and (2) it takes approximately one month for R to exit the drainage system, aligning with the monthly time step of GRACE/FO data. Note that total runoff from Ghiggi et al. (2021) stopped in 2019, and we used monthly climatology values between 2002 and 2019 to extend the data to 2022 and align with the GRACE/FO record length. Other contributions to TWS drawdowns, such as changes in water intercepted by leaf and branch surfaces and internal plant water storage, are too small to be detected by GRACE/FO (Rodell et al., 2005) and unlikely to significantly affect our estimates. Our method also implicitly includes moisture stored in the topsoil for soil evaporation (Stoy et al., 2019). However, the contribution of soil evaporation to ET decreases quickly as TWS draws down (Stocker et al., 2023), and we expect that the magnitude of the largest drawdown will be determined by root-zone depletion magnitude reflected at the end of the drawdown.

We calculated the random error of $S_r^{GRACE/FO}$ by adding errors of the two GRACE/FO measurements and the uncertainty of groundwater pumping and surface water signals in quadrature. To calculate the GRACE/FO measurement error, we used the formal error product provided by the JPL mascon solutions (Watkins et al., 2015; Wiese et al., 2016). For the uncertainty of groundwater pumping and surface water signals, we assumed a $\pm 50\%$ error on the magnitude of our calculated signals, following Zhao et al. (2021). This assumption implies that the uncertainty range is equal to the signals themselves, leading to a likely conservative error estimate.

116 2.3 Comparison to other S_r estimates

117 We compared our $S_r^{GRACE/FO}$ estimate to two other S_r datasets. These datasets represent the typical rooting depth \times soil
118 texture-dependent water holding capacity approach (referred to as $S_r^{RD \times WHC}$) and the water deficit accumulation approach
119 (referred to as S_r^{accum}). We chose the S_r^{accum} estimate from Stocker et al. (2023) because it used the latest Earth observation-
120 constrained estimates of precipitation and evapotranspiration. We used their “SCWD_{X80}” product which was estimated based on
121 cumulative water deficit extremes occurring with a return period of 80 years. We calculated $S_r^{RD \times WHC}$ using existing datasets
122 on rooting depths and soil texture. The $RD \times WHC$ approach requires knowing effective rooting depths (Federer et al., 2003;
123 Speich et al., 2018; Stocker et al., 2023; Bachofen et al., 2024). We obtained effective rooting depths from Yang et al. (2016),
124 who derived them using an analytical model that balances the marginal carbon cost and benefits of deeper roots. While such
125 model-based datasets are valuable for providing comprehensive coverage and insights into complex processes, they do not
126 incorporate direct observational data for validation or correction. Soil water holding capacity, defined as the difference between
127 field capacity and permanent wilting point, is calculated based on soil texture information from the Harmonized World Soil
128 Database version 1.2 (Wieder et al., 2014) and pedo-transfer functions based on Balland et al. (2008). The Harmonized World
129 Soil Database provides information for depths of 0-0.3 m and 0.3-1 m. For depths greater than 1 m, we assume texture values
130 from the 0.3-1 m depth following Stocker et al. (2023). For consistency, we spatially averaged both S_r^{accum} and $S_r^{RD \times WHC}$
131 estimates to match the GRACE/FO spatial scale ($3^\circ \times 3^\circ$).

132 2.4 Evaluation using the USGS monthly hydrologic model

133 Validating large-scale S_r remains inherently difficult because direct measurement of S_r is challenging. Previous studies
134 have primarily employed two indirect methods: comparison to measured rooting depths and hydrological modelling. Stocker
135 et al. (2023) converted their deficit-based S_r estimates (~ 5 km resolution) into rooting depths using soil texture and water-
136 holding capacity parameters and then compared them to field rooting depth measurements aggregated at biome levels to
137 mitigate the scale mismatch. However, this approach is not suitable for our study as GRACE/FO-derived S_r (~ 300 km)
138 encompasses multiple biome types within the effective resolution of GRACE/FO data, making biome-level aggregation less
139 meaningful. Additionally, the rooting depth method overlooks groundwater and rock moisture contributions to S_r , which
140 Stocker et al. (2023) found to be significant in over half of their root measurement sites. This omission will likely become
141 more critical at the spatial scale of GRACE/FO, which averages larger areas and includes more diverse biome types. These
142 factors make the rooting depth comparison unsuitable for evaluating GRACE/FO-derived S_r . Wang-Erlandsson et al. (2016)
143 used deficit-based S_r estimates in a simple hydrological model and assessed improvements in simulating hydrologic time series.
144 While this approach better aligns with the scale of GRACE/FO, it is constrained by the limited availability of high-quality
145 global hydrologic data. This can lead to a circular use of the same data for both S_r estimation and model evaluation, as seen
146 when Wang-Erlandsson et al. (2016) used satellite-based ET data for both S_r estimation and model evaluation, reducing the

147 independence of the validation process. We also noted that existing gridded ET products generally have assumed ecosystem
 148 responses to water stress in their algorithms and are thus highly uncertain (Miralles et al., 2016).

149 To address these challenges, we evaluated the relative accuracy of $S_r^{GRACE/FO}$, S_r^{accum} and $S_r^{RD \times WHC}$ by separately
 150 parameterizing a hydrological model with each estimate, referred to as *HydroModel*($S_r^{GRACE/FO}$), *HydroModel*(S_r^{accum}), and
 151 *HydroModel*($S_r^{RD \times WHC}$). We then assessed their accuracy in simulating ET using an independent dataset: version 4.1 of the
 152 Global Land Evaporation Amsterdam Model (GLEAM) ET (Miralles et al., 2024). This dataset was not involved in the
 153 calculation of $S_r^{GRACE/FO}$, S_r^{accum} , or $S_r^{RD \times WHC}$, ensuring independence and avoiding circular validation that affected previous
 154 studies (e.g., Wang-Erlandsson et al., 2016). Furthermore, the GLEAM ET product provides several key improvements over
 155 other gridded ET products. For example, it combines hybrid learning from eddy-covariance and sap flow to better capture
 156 vegetation response to drought (Koppa et al., 2022) and explicitly accounts for plant access to groundwater (Hulsman et al.,
 157 2023). The atmospheric forcing data and model parameters were identical across simulations, with S_r being the only variable
 158 parameter. Therefore, differences in model performance reflect the relative accuracy of the three S_r estimates. A monthly
 159 hydrologic model developed by the United States Geological Survey (USGS) (McCabe and Markstrom, 2007) was used due
 160 to its simplicity and transparency about physical processes. Specifically, the model relies on a straightforward specification of
 161 S_r as a “water bucket” depth rather than indirectly through prescribed rooting depth, soil texture, and pedo-transfer functions
 162 across the profile. This allows us to parameterize the model directly with $S_r^{GRACE/FO}$, S_r^{accum} , and $S_r^{RD \times WHC}$. The USGS model
 163 was run at each GRACE mascon location with air temperature forcing from ERA5 and precipitation forcing from GPCP. We
 164 used climate forcing from 1993 to 2001 to spin up the model and performed water cycle simulations for the study period from
 165 2002 to 2022. No calibrations were carried out.

166 To mitigate the impact of possible biases embedded in GLEAM ET, the forcing data, and those caused by model
 167 uncertainty (as the USGS model is uncalibrated), we used standardized ET anomalies (i.e., Z-scores) as the target of validation
 168 and focused on assessing whether S_r improves the temporal dynamics of ET simulations (i.e., seasonal and interannual
 169 variations) rather than the absolute values of ET. The Nash-Sutcliffe model efficiency (NSE) coefficient was used to assess
 170 the predictive skill of each USGS hydrologic model, which is defined as:

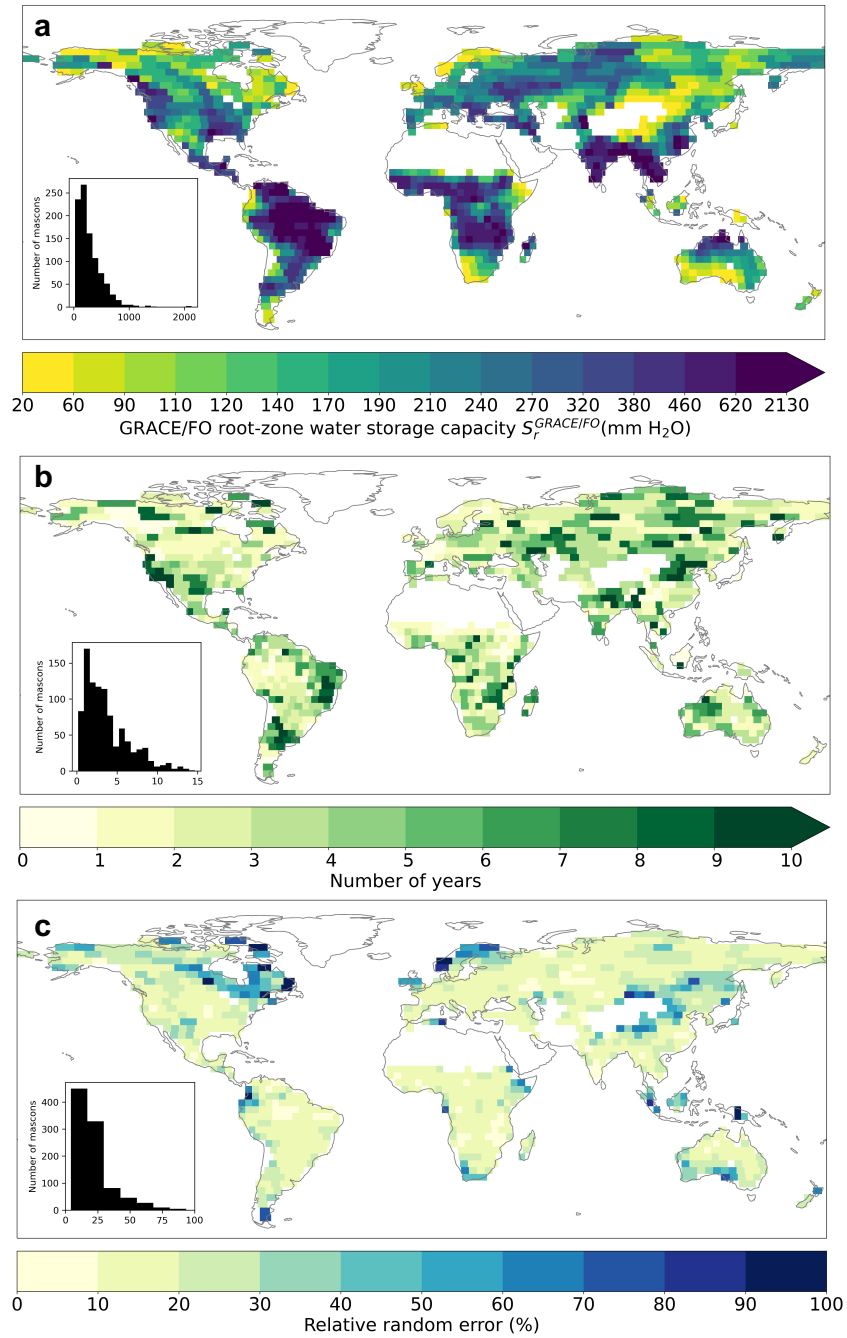
$$NSE = 1 - \frac{\sum_{t=1}^T (X_o^t - X_m^t)^2}{\sum_{t=1}^T (X_o^t - \overline{X_o})^2} \quad (2)$$

171 where X represents the standardized ET anomaly, $\overline{X_o}$ is the mean of observed X , and X_o^t and X_m^t are observed and modeled X
 172 at time t , respectively (Nash and Sutcliffe, 1970). An NSE value closer to 1 indicates a better model performance in simulating
 173 X , while an NSE value less than 0 indicates that the mean observed value is a better predictor than the simulated value,
 174 suggesting an unsatisfactory model performance (Nash and Sutcliffe, 1970). If *HydroModel*($S_r^{GRACE/FO}$), *HydroModel*(S_r^{accum}),
 175 and *HydroModel*($S_r^{RD \times WHC}$) all yield negative NSE values, the efficacy of using the USGS hydrologic model to evaluate the
 176 relative accuracy of the three S_r estimates is compromised.

177 3 Results

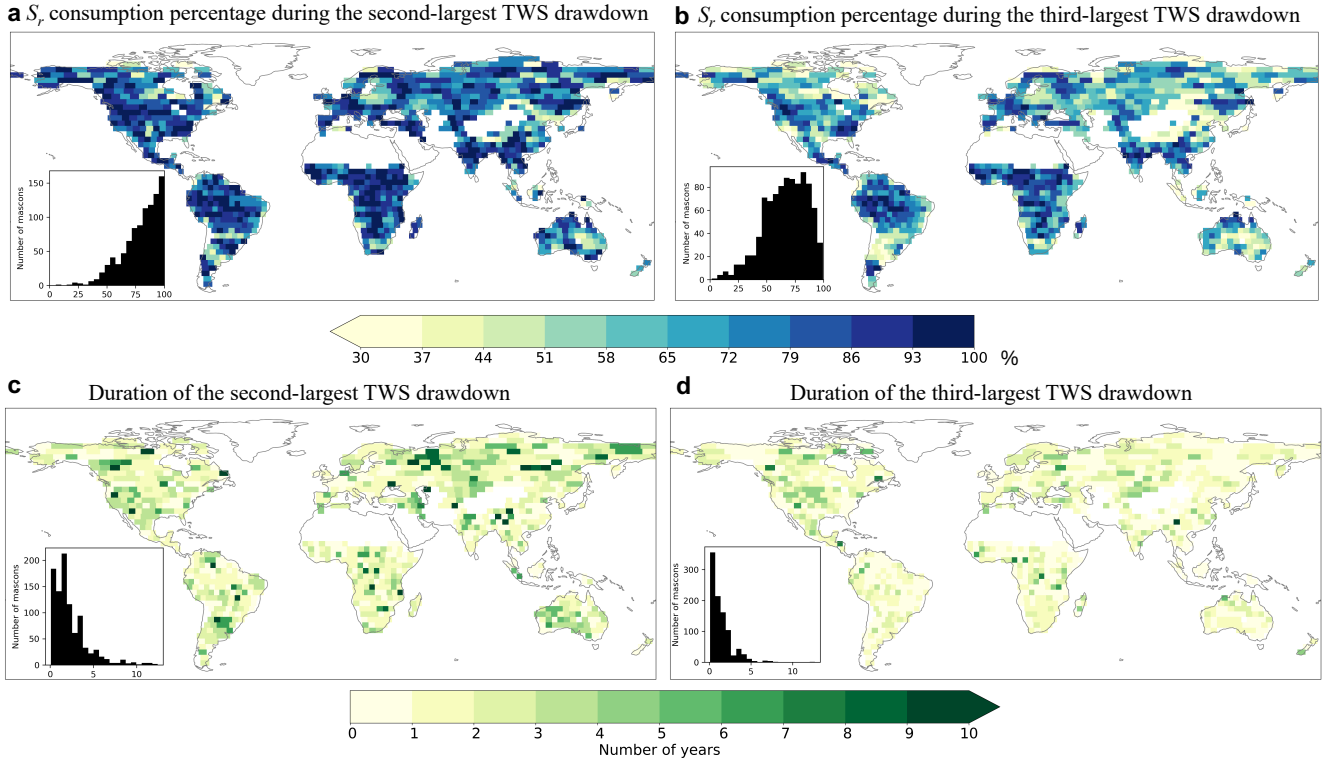
178 3.1 S_r from GRACE/FO ($S_r^{GRACE/FO}$)

179 We find a substantial root-zone water storage capacity worldwide. Across the global vegetated domain, $S_r^{GRACE/FO}$ (or
180 the largest TWS drawdown) spans from 22 to 2131 mm (Fig. 2a). The distribution of $S_r^{GRACE/FO}$ is positively skewed, with a
181 median value of 221 mm (129 - 389 mm interquartile range; note that values in parentheses hereafter always refer to the
182 interquartile range). Larger $S_r^{GRACE/FO}$ are associated with densely vegetated regions like the tropical rainforests, the
183 Southeastern U.S., the Pacific Northwest, and the southern part of China. By contrast, smaller $S_r^{GRACE/FO}$ are found in sparsely
184 vegetated regions like Central Asia, much of Australia, and some Arctic regions (Fig. 2a). Fig. 2b shows the duration of the
185 maximum TWS drawdown with a global median of 2.8 years (1.6 - 5.2 years). We find no correlation between the duration
186 and the magnitude of the largest TWS drawdown across different regions (Figs. 2a-b). The impact of random error sources on
187 our $S_r^{GRACE/FO}$ estimate remains moderate, with a global median relative error of 18% (13% - 26%) (Fig. 2c).



188
 189 **Figure 2.** S_r estimated from GRACE/FO total water storage (TWS) anomaly. (a) Global patterns of $S_r^{GRACE/FO}$ for Earth's
 190 vegetated regions. (b) The duration of the maximum TWS drawdown. (c) Global patterns of the random error of $S_r^{GRACE/FO}$.
 191 Insets in (a) - (c) show the histograms of corresponding mapping variables across our study area. White spaces on land represent
 192 mascon locations with less than 50% vegetation cover.

193 To characterize the utilization of root-zone water storage capacity, we compared the second and third-largest TWS
 194 drawdowns to $S_r^{GRACE/FO}$. We find that, on average, the second-largest TWS drawdown consumes 83% (71% - 92%) of the
 195 $S_r^{GRACE/FO}$ estimate (Fig. 3a), while the third-largest uses 68% (54% - 82%) (Fig. 3b). The average duration of the second- and
 196 third-largest TWS drawdowns decreases from 1.6 years (1.1 - 3.2 years) to 1.2 years (0.5 - 1.7 years) (Figs. 3c-d). In about
 197 40% of our analysed mascons, the longest TWS drawdown period does not coincide with the largest drawdown magnitude.
 198 These findings underscore the nuanced dynamics of water storage use within the root zone, suggesting variability in both
 199 magnitude and duration across different regions.
 200

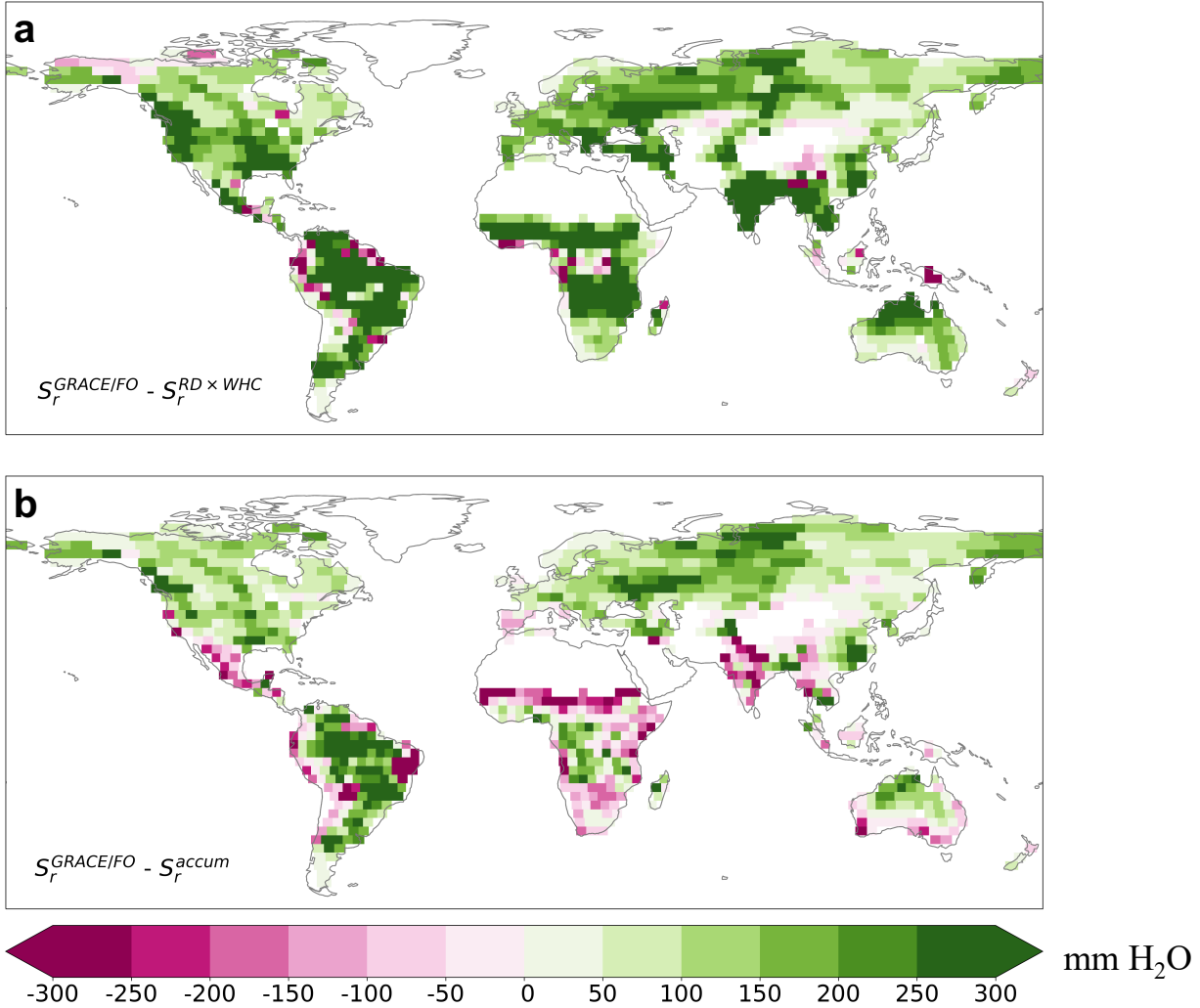


201
 202 **Figure 3.** Utilization of root zone water storage capacity. (a) and (b) are consumption percentages of $S_r^{GRACE/FO}$ during the
 203 second and third-largest TWS drawdowns. (c) and (d) are the duration of the second and third-largest TWS drawdowns. Insets
 204 in (a) - (d) show the histograms of corresponding mapped variables.

205 3.2 Comparison with other S_r estimates

206 Our $S_r^{GRACE/FO}$ estimate is larger than $S_r^{RD \times WHC}$ and S_r^{accum} over much of the globe. Figs. 4a-b show $S_r^{GRACE/FO}$ difference
 207 with $S_r^{RD \times WHC}$ and S_r^{accum} , respectively. Across the global vegetated domain, $S_r^{GRACE/FO}$ surpasses $S_r^{RD \times WHC}$ in over 90% of
 208 mascon locations, with a median value 175 mm (or 380%) higher than that of $S_r^{RD \times WHC}$. The $S_r^{GRACE/FO}$ exceeds S_r^{accum} over
 209 70% of the study area, with a median value 77 mm (or 53%) higher than that of S_r^{accum} , despite exhibiting lower values in

210 many regions of Africa, India, Mexico, and northeast Brazil (Fig. 4b). Notably, these differences are greater than the random
 211 error of $S_r^{GRACE/FO}$, emphasizing that the underestimations by $S_r^{RD \times WHC}$ and S_r^{accum} are significant.



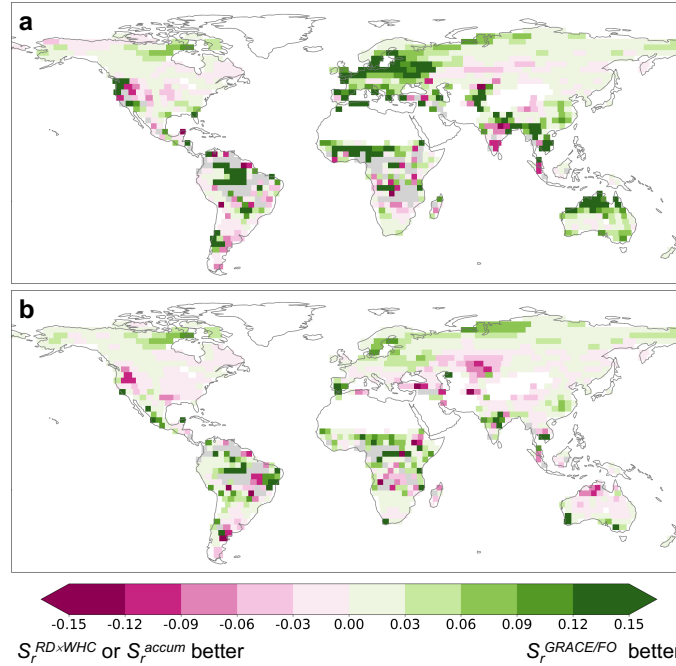
212 -300 -250 -200 -150 -100 -50 0 50 100 150 200 250 300 mm H₂O
 213 **Figure 4.** $S_r^{GRACE/FO}$ is notably larger than other datasets over much of the globe. (a) The difference between $S_r^{GRACE/FO}$ and
 214 $S_r^{RD \times WHC}$. (b) The difference between $S_r^{GRACE/FO}$ and S_r^{accum} .

215 3.3 Implementation in the USGS hydrologic model

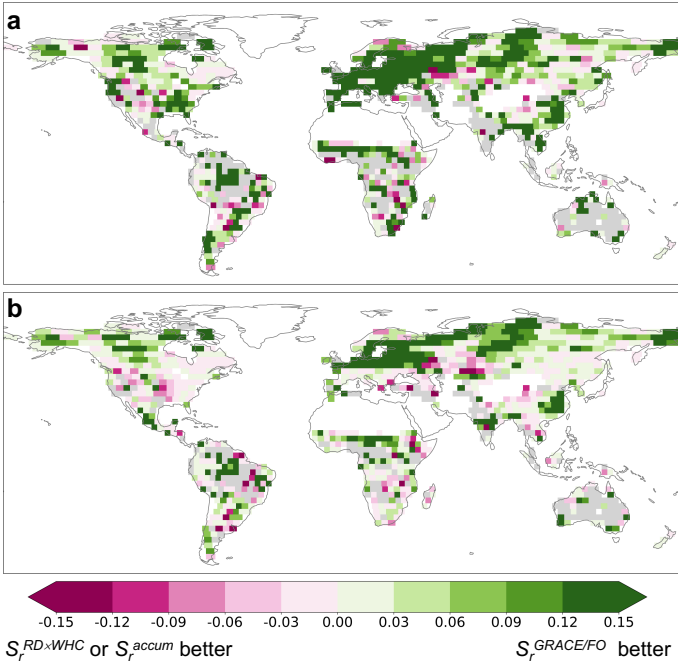
216 To assess whether $S_r^{GRACE/FO}$ is an improvement over S_r^{accum} and $S_r^{RD \times WHC}$, we used each of them to separately
 217 parameterize the USGS hydrologic model. We first evaluated the accuracy of $HydroModel(S_r^{GRACE/FO})$, $HydroModel(S_r^{RD \times WHC})$,
 218 and $HydroModel(S_r^{accum})$ in replicating the full time series of standardized GLEAM ET anomalies. For over 95% of the global
 219 vegetated domain, at least one model achieved a positive NSE value. In these regions, the average NSE for
 220 $HydroModel(S_r^{GRACE/FO})$ is 0.73 (0.65 - 0.89), for $HydroModel(S_r^{RD \times WHC})$ it is 0.69 (0.63 - 0.86), for $HydroModel(S_r^{accum})$ it is

221 0.72 (0.64 - 0.87). These relatively high NSE values indicate the USGS model is effective in simulating ET. While the global
 222 average NSE values for the three models are similar, $HydroModel(S_r^{GRACE/FO})$ demonstrates slightly superior performance,
 223 outperforming $HydroModel(S_r^{RD \times WHC})$ in 66% of the vegetated regions and $HydroModel(S_r^{accum})$ in 59% of these regions (Fig.
 224 5).

225 We hypothesized that a more accurate S_r would have a greater impact on improving ET simulations during drought
 226 periods when ET is more dependent on deep subsurface water storage. To test this, we calculated NSE values specifically for
 227 drought periods, defined as when the 3-month standardized precipitation index was less than -1.2, indicative of severe drought
 228 conditions (McKee et al., 1993). Across 87% of the global vegetated domain, at least one model achieved a positive NSE
 229 value. In these regions, the average NSE for $HydroModel(S_r^{GRACE/FO})$ is 0.65 (0.52 - 0.86), for $HydroModel(S_r^{RD \times WHC})$ it is 0.52
 230 (0.40 - 0.81), for $HydroModel(S_r^{accum})$ it is 0.61 (0.48 - 0.84). These lower NSE values compared to the full ET time series
 231 reflect the challenges faced by the USGS model in simulating ET during droughts, consistent with previous findings (e.g.,
 232 Zhao et al., 2022). However, $HydroModel(S_r^{GRACE/FO})$ showed notable improvement over the other two models, particularly in
 233 high-latitude regions (Fig. 6). These results suggest that while $S_r^{GRACE/FO}$ provides only marginal improvements for the full
 234 time series of standardized GLEAM ET anomalies, its superiority over $S_r^{RD \times WHC}$ and S_r^{accum} becomes more pronounced during
 235 drought conditions.



236 **Figure 5.** $S_r^{GRACE/FO}$ improves overall model performance in simulating standardized ET anomalies over much of the globe.
 237 (a) The NSE difference between $HydroModel(S_r^{GRACE/FO})$ and $HydroModel(S_r^{RD \times WHC})$ for full time series. (b) The NSE
 238 difference between $HydroModel(S_r^{GRACE/FO})$ and $HydroModel(S_r^{accum})$ for full time series. Gray areas indicate regions where
 239 all models fail to achieve a positive NSE value.
 240



242

243 **Figure 6.** $S_r^{GRACE/FO}$ notably improves model performance in simulating standardized ET anomalies during drought periods
244 across much of the globe. (a) and (b) are similar to Figs. 5a and 5b, respectively, except for drought time periods. Gray areas
245 indicate regions where all models fail to achieve a positive NSE value.

246 **4 Discussion**

247 **4.1 Limitations and uncertainty in $S_r^{GRACE/FO}$**

248 Our $S_r^{GRACE/FO}$ estimate provides a conservative lower bound on S_r because the largest TWS drawdown during the
249 GRACE/FO record period may not cover a period during which ET from storage exhausts the entire root-zone water storage
250 capacity, particularly in areas experiencing water accumulation in the root zone due to increases in precipitation. This likely
251 explains why our $S_r^{GRACE/FO}$ estimate is lower than S_r^{accum} in North and East Africa, where strong increasing TWS trends were
252 observed (Fig. 3b and Fig. A2) in response to increasing precipitation trends (e.g., Rodell et al., 2018). Additionally, our
253 approach to account for groundwater pumping and surface water may overestimate these signals' actual magnitudes and thus
254 likely contribute to underestimating S_r . Specifically, we assumed all negative TWS trends to be caused by groundwater
255 withdrawals and removed them from $S_r^{GRACE/FO}$. However, intense groundwater withdrawals are concentrated in specific
256 regions such as northwest India, California's Central Valley, and the North China Plain (Rodell et al., 2009; Feng et al., 2013;
257 Liu et al., 2022). Consequently, we may have removed TWS depletion trends caused by natural variability, as seen in the
258 drought-stricken Southeast Brazil (Rodell et al., 2018). This likely explains why $S_r^{GRACE/FO}$ is lower than S_r^{accum} there (Fig. 3b).

Furthermore, we used total runoff (which includes surface runoff, snowmelt, and groundwater discharge) as a proxy to remove surface water storage change from the TWS drawdown. We used total runoff – as opposed to surface runoff alone (Wang et al., 2023a) – due to observational data availability, though doing so may lead to an overestimation of surface water storage change and, therefore, an underestimation of S_r .

4.2 $S_r^{GRACE/FO}$ vs. S_r^{accum} : impact of multi-year drawdowns and drought return period assumption

Despite being conservative, $S_r^{GRACE/FO}$ reveals a substantially larger volume of root-zone water storage capacity than S_r^{accum} . One reason for this discrepancy may be the lack of interannual storage variability considered in the S_r^{accum} calculation (Stocker et al., 2023). Although Stocker et al. (2023) used a cumulative water deficit approach to infer root-zone water storage drawdown, akin to our TWS drawdown approach, they found that the annual totals of P exceeded those of ET at almost all locations. Because their method resets the calculation whenever accumulated P-ET is positive, this suggests their method generally was unable to account for carryover storage and multiyear drawdowns of root-zone storage. Our use of GRACE/FO TWS, which allows for multiyear drawdowns, is supported by recent observations (Goulden and Bales, 2019; McCormick et al., 2021; Pérez-Ruiz et al., 2022; Peterson et al., 2021; Scott and Biederman, 2019) and modelling efforts (Miguez-Macho and Fan, 2021; Livneh and Hoerling, 2016) suggesting widespread carryover storage effects. Our calculations of $S_r^{GRACE/FO}$ found that the largest TWS drawdown period lasted a median of 2.8 years, with an interquartile range between 1.6 and 5.2 years (Fig. 2c). Even the second and third-largest TWS drawdowns had a median duration of more than one year globally (Figs. 3c-d). These findings align with the results reported in the previously referenced studies on carryover storage effects.

The discrepancy between $S_r^{GRACE/FO}$ and S_r^{accum} is further influenced by differences in how drought return periods are defined. S_r^{accum} values reported in Stocker et al. (2023) are statistically scaled to represent an 80-year drought return period, rather than being directly derived from observed drought events. This extrapolation assumes a fixed probability distribution of drought occurrence, which may not fully capture real-world hydrological variability. In contrast, $S_r^{GRACE/FO}$ is based on observed multiyear TWS drawdowns from 2002-2022, directly reflecting droughts that occurred over the past two decades. A more comparable approach would require using the unscaled S_r^{accum} , which was derived using Earth observations of precipitation and ET from 2003-2018, without statistical adjustments. However, the unscaled S_r^{accum} is not publicly available. Given that the 80-year return period scaling inflates S_r^{accum} values, and $S_r^{GRACE/FO}$ is still substantially larger, it follows that the unscaled S_r^{accum} would be even lower, further supporting the conclusion that the S_r^{accum} approach underestimates root-zone storage capacity compared to $S_r^{GRACE/FO}$.

4.3 Groundwater and rock moisture in $S_r^{GRACE/FO}$ and differences with $S_r^{RD \times WHC}$

The $S_r^{RD \times WHC}$ estimate notably falls below both $S_r^{GRACE/FO}$ and S_r^{accum} . This discrepancy may be attributed to the $RD \times WHC$ approach ignoring plant access to moisture stored beneath the soil, such as in weathered and fractured bedrock and groundwater. These deep moisture sources are known to significantly affect ET and thus contribute to S_r (e.g., Fan et al., 2017;

290 Rempe and Dietrich, 2018; McCormick et al., 2021). Unlike $S_r^{RD \times WHC}$, the definitions of $S_r^{GRACE/FO}$ and S_r^{accum} incorporate
 291 natural variability in these deep moisture reserves, broadening the traditional “root zone” concept beyond the unsaturated soil
 292 layer. This expanded definition acknowledges the dynamic nature of the root zone, with plants accessing deep groundwater
 293 and rock moisture during prolonged droughts and periods of high transpiration demand (Gao et al., 2024). Indeed, root-
 294 accessible water does not require roots to physically occupy the entire storage domain. Processes like capillary rise can move
 295 deep water upward to the traditional “root zone” for vegetation transpiration, especially during dry seasons and droughts.

296 The importance of including groundwater and rock moisture in S_r is well-supported by recent evidence. Studies using
 297 *in situ* groundwater (Fan et al., 2017; Thompson et al., 2011; Baldocchi et al., 2021; Li et al., 2015), remote sensing
 298 observations (Koirala et al., 2017; Rohde et al., 2024), and modeling efforts (Miguez-Macho and Fan, 2021; Hain et al., 2015)
 299 have demonstrated that plants can access these deep moisture sources and highlighted their critical role in sustaining ET,
 300 especially during extreme droughts. In many ecosystems, water stress can stimulate root growth into deep subsurface through
 301 the capillary rise effect, with roots extending to the capillary fringe and the water table, as observed in both field and laboratory
 302 studies (Naumburg et al., 2005; Orellana et al., 2012; Fan et al., 2017; Kuzyakov and Razavi, 2019). Although individual
 303 shallow-rooted plants (e.g., grassland sites) may not directly tap into groundwater or rock moisture, the large spatial scale of
 304 GRACE/FO likely captures water uptake across diverse vegetation types. Even in areas primarily covered by shallow-rooted
 305 vegetation, deeper-rooted plants within the same GRACE/FO mascon may redistribute water upward through hydraulic
 306 redistribution, making it available for shallow-rooted plants to use (e.g., Espeleta et al., 2004; Orellana et al., 2012). In fact,
 307 satellite observations have confirmed widespread plant-groundwater interactions at large spatial scales (Koirala et al., 2017),
 308 even in dryland regions dominated by grasslands (Rohde et al., 2024; Wang et al., 2023b). Recognizing and incorporating
 309 groundwater and bedrock moisture in root zone storage capacity can enhance our understanding of land-atmosphere
 310 interactions (Maxwell and Condon, 2016; Schlemmer et al., 2018; Dong et al., 2022), improve runoff simulations (Hahm et
 311 al., 2019), and provide a more accurate representation of vegetation resilience to droughts and heat waves (Jiménez-Rodríguez
 312 et al., 2022; Esteban et al., 2021).

313 The $RD \times WHC$ approach, while useful for simplifying root zone complexity, overlooks critical aspects of root density,
 314 its vertical and lateral distribution, and the ability of plants to access deep water stores – factors that have significant
 315 implications for understanding ecosystem water uptake and improving land models. For instance, this approach reduces the
 316 complexity of rooting systems into a single effective rooting depth parameter (Federer et al., 2003; Speich et al., 2018), which
 317 tends to be shallower than both the maximum rooting depth (Federer et al., 2003) and the depth that contains the upper 95%
 318 of the root biomass (Yang et al., 2016). These deeper layers, however, often play a disproportionately important role in
 319 ecosystem water uptake (Fan et al., 2017; Jackson et al., 1999; Bachofen et al., 2024). Additionally, when dividing $S_r^{GRACE/FO}$
 320 with the same WHC used in $S_r^{RD \times WHC}$ to calculate effective rooting depth, this depth exceeds 2 m in nearly 50% of global
 321 vegetated areas, in contrast to Yang et al.’s (2016) estimate of 10% and Stocker et al.’s (2023) estimate of 37%. These results
 322 indicate that the potential for plants to tap into deep water stores is more prevalent than previously understood. For land models
 323 that do not explicitly incorporate S_r as a variable, this suggests that models with a soil depth of less than 2 m (e.g., the Noah

324 model within the Global Land Data Assimilation System (GLDAS)) may be unable to accurately simulate these deeper water
325 drawdowns. Consequently, this limitation could impact studies of groundwater that rely on GLDAS to separate soil moisture
326 from TWS (e.g., Rodell et al., 2009).

327 4.4 Strengths and limitations of $S_r^{GRACE/FO}$ validation

328 Although direct observations of S_r at large spatial scales are limited, our validation effort for $S_r^{GRACE/FO}$ shows two
329 notable strengths. First, we used an independent dataset for the validation of USGS models parameterized by different S_r
330 estimates, unlike a previous study (Wang-Erlandsson et al., 2016), which relied on a dataset already used in their S_r calculation.
331 Second, the GLEAM ET dataset used here for validation addresses key limitations of other gridded ET products by using a
332 data-driven embedding of plant-water relationships (rather than explicitly assuming these a priori as most ET products do) and
333 explicitly accounting for groundwater contributions to ET (Miralles et al., 2024).

334 Despite these strengths, our validation effort is not without limitations. First, the mechanistic linkage between S_r and
335 commonly used hydrological indicators (e.g., ET and streamflow) is complex. Identifying decisive indicators that are highly
336 sensitive to S_r is an ongoing research challenge. In this context, our findings provide an initial step towards understanding this
337 relationship, demonstrating that a more accurate S_r improves simulations of drought-time ET anomalies more effectively than
338 all-time variations (Figs. 5 and 6). However, resolving such a complex relationship is further complicated by model structural
339 errors or uncertainties in other model parameters, which can obscure the true impact of accurate S_r parameterization on
340 ecohydrological processes. For example, in our study, streamflow simulated by the USGS model is mainly driven by
341 precipitation and shows limited sensitivity to S_r (results not shown). This aligns with the findings of another simple hydrologic
342 model used by Wang-Erlandsson et al. (2016), as discussed in their open peer review file, where streamflow measurements
343 were also not used for model evaluation. Second, we used standardized ET anomalies (Z-scores) as the validation target,
344 focusing on temporal dynamics such as seasonal and interannual variations rather than absolute ET values. While this approach
345 effectively mitigates the impact of data biases and ensures consistency, it narrows the scope of the validation.

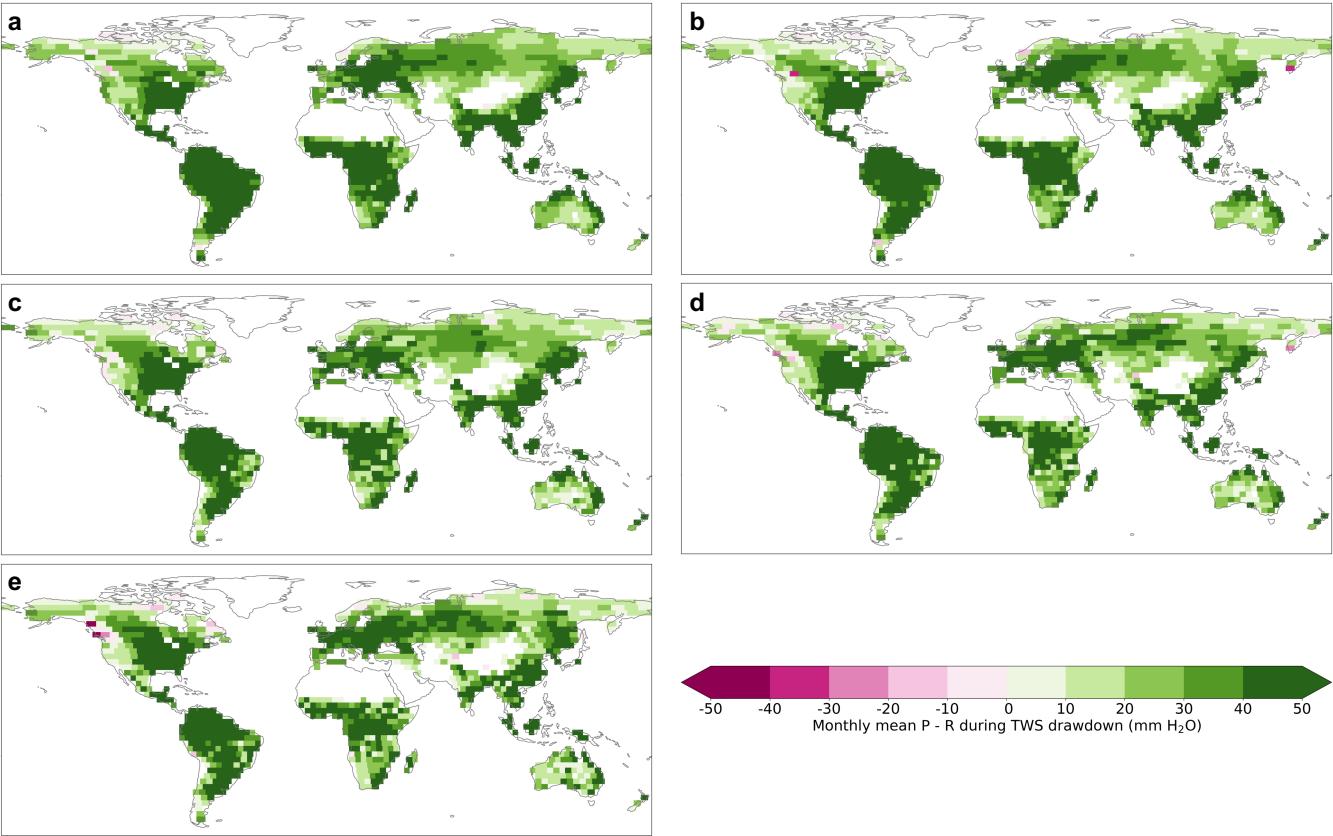
346 4.5 Implications for high-resolution land surface models

347 Despite the coarse resolution of GRACE/FO observations, $S_r^{GRACE/FO}$ and our proposed approach remain valuable for
348 improving the operational configuration of higher-resolution land models. First, $S_r^{GRACE/FO}$ can be used to evaluate and refine
349 default S_r parameterizations within models once aggregated to coarse scale of GRACE/FO data, in conjunction with other
350 diagnostic analyses. For instance, if a model underestimates ET during droughts in a region where its S_r value is significantly
351 lower than $S_r^{GRACE/FO}$, the default S_r value may be increased based on $S_r^{GRACE/FO}$ even if the model's resolution is much higher
352 than that of $S_r^{GRACE/FO}$. Second, in the future, our methodology can be extended to downscaled GRACE/FO products, leveraging
353 techniques such as data assimilation systems or artificial intelligence to improve the spatial resolution of $S_r^{GRACE/FO}$ (Li et al.,
354 2019; Gou and Soja, 2024).

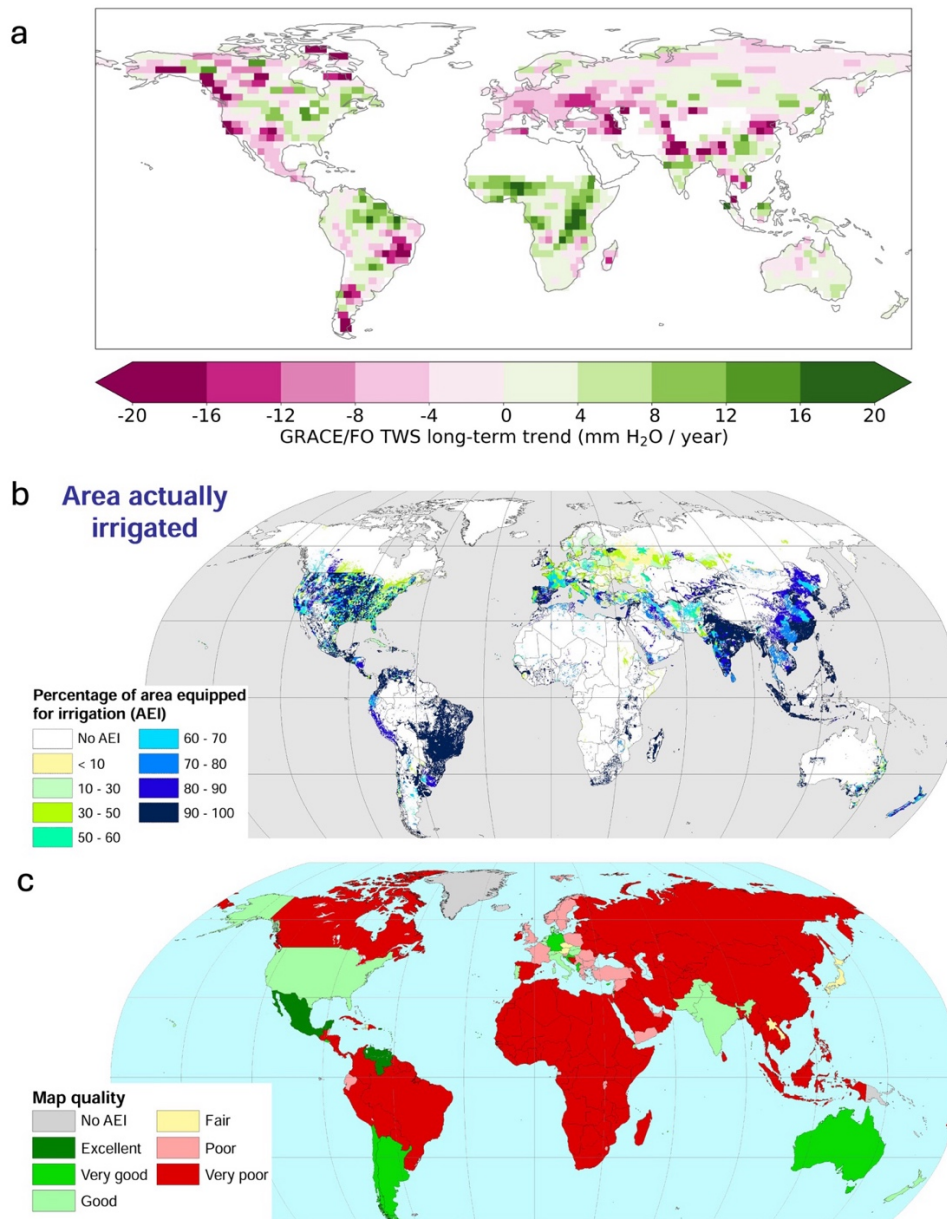
355 **5 Conclusions**

356 We used GRACE/FO TWS observations to estimate root-zone water storage capacity (S_r), an essential yet
357 challenging-to-observe variable. The overall improved performance of *HydroModel*($S_r^{GRACE/FO}$) in simulating ET, particularly
358 during droughts, implies that $S_r^{GRACE/FO}$ more accurately reflects the real-world root-zone water storage capacity compared to
359 $S_r^{RD \times WHC}$ and S_r^{accum} . Overall, our results suggest that S_r is, on average, at least 50% larger than the water deficit-based estimate
360 and by a staggering 380% compared to the rooting depth-based estimate. The underestimations by S_r^{accum} and $S_r^{RD \times WHC}$ exceed
361 the random error of $S_r^{GRACE/FO}$, underscoring the need for continued refinement and validation of S_r . Underestimating S_r may
362 lead to overestimating ecosystem sensitivity to water stress, potentially biasing predictions of future carbon cycle (Ukkola et
363 al., 2021; Giardina et al., 2023). Given the strong coupling between the carbon and water cycles, underestimating S_r may also
364 lead to underestimating ecosystem water consumption and overestimating human-available water resources, particularly
365 during droughts and heat waves, with important implications for water resource planning (Zhao et al., 2022; Mastrotheodoros
366 et al., 2020).

367



369
370 **Figure A1.** The average P - R during the largest (a), the second largest (b), the third largest (c), the fourth largest (d), and the
371 fifth largest (e) TWS drawdowns.
372



373
 374 **Figure A2.** (a) Trends in TWS obtained from GRACE/FO observations from 2002 to 2022. (b) Percentage of area equipped
 375 for irrigation that is actually irrigated. (c) Map quality marks assigned to each country for area equipped for irrigation in (b).
 376 (b-c) are from the Global Map of Irrigation Areas – version 5.0 by AQUASTA.

377 Code availability

378 The Python code for retrieving S_r from GRACE/FO is archived on Zenodo at <https://doi.org/10.5281/zenodo.14970062>.

379 **Data availability**

380 The $S_r^{GRACE/FO}$ dataset is archived on Zenodo at <https://doi.org/10.5281/zenodo.14970062>. GRACE and GRACE-FO TWS data
381 are available from the NASA JPL (https://grace.jpl.nasa.gov/data/get-data/jpl_global_mascons/). The GPCP version 2.3
382 combined precipitation dataset is available at <https://psl.noaa.gov/data/gridded/data.gpcp.html>. ERA5 reanalysis is available
383 at <https://www.ecmwf.int/en/forecasts/datasets/reanalysis-datasets/era5>. MODIS land cover data are available
384 at <https://lpdaac.usgs.gov/products/mcd12c1v006/>. Water-balance-based ET data is available at
385 <https://doi.org/10.5281/zenodo.8339655>. G-RUN global runoff reconstruction data is available at
386 https://figshare.com/articles/dataset/GRUN_Global_Runoff_Reconstruction/9228176. GLEAM ET version 4.1 is available at
387 <https://www.gleam.eu/>.

388 **Author contribution**

389 MZ: Conceptualization; Data curation; Formal analysis; Funding acquisition; Methodology; Writing - original draft. ELM:
390 Methodology; Writing - review & editing. GA: Methodology; Writing - review & editing. AGK: Writing - review & editing.
391 BL: Writing - review & editing.

392 **Competing interest**

393 The authors declare that they have no conflict of interest.

394 **Acknowledgments**

395 This study was funded by the USGS grant G24AP00031 to the University of Idaho. In addition, ELM was funded by the NSF
396 Graduate Research Fellowship program and AGK was funded by the NSF DEB 1942133 and the Alfred P. Solan Foundation.

397 **References**

398 Bachofen, C., Tumber-Dávila, S. J., Mackay, D. S., McDowell, N. G., Carminati, A., Klein, T., Stocker, B. D., Mencuccini,
399 M., and Grossiord, C.: Tree water uptake patterns across the globe, *New Phytologist*, 242, 1891-1910,
400 <https://doi.org/10.1111/nph.19762>, 2024.

401 Baldocchi, D., Ma, S., and Verfaillie, J.: On the inter- and intra-annual variability of ecosystem evapotranspiration and water
402 use efficiency of an oak savanna and annual grassland subjected to booms and busts in rainfall, *Global Change Biology*, 27,
403 359-375, <https://doi.org/10.1111/gcb.15414>, 2021.

404 Balland, V., Pollacco, J. A., and Arp, P. A.: Modeling soil hydraulic properties for a wide range of soil conditions, *Ecological*
405 *Modelling*, 219, 300-316, 2008.

406 Callahan, R. P., Riebe, C. S., Sklar, L. S., Pasquet, S., Ferrier, K. L., Hahm, W. J., Taylor, N. J., Grana, D., Flinchum, B. A.,
407 and Hayes, J. L.: Forest vulnerability to drought controlled by bedrock composition, *Nature Geoscience*, 15, 714-719, 2022.

408 Chen, Y., Velicogna, I., Famiglietti, J. S., and Randerson, J. T.: Satellite observations of terrestrial water storage provide early
409 warning information about drought and fire season severity in the Amazon, *Journal of Geophysical Research: Biogeosciences*,
410 118, 495-504, <https://doi.org/10.1002/jgrg.20046>, 2013.

411 Dong, J., Lei, F., and Crow, W. T.: Land transpiration-evaporation partitioning errors responsible for modeled summertime
412 warm bias in the central United States, *Nature Communications*, 13, 336, 10.1038/s41467-021-27938-6, 2022.

413 Espeleta, J. F., West, J. B., and Donovan, L. A.: Species-specific patterns of hydraulic lift in co-occurring adult trees and
414 grasses in a sandhill community, *Oecologia*, 138, 341-349, 10.1007/s00442-003-1460-8, 2004.

415 Esteban, E. J. L., Castilho, C. V., Melgaço, K. L., and Costa, F. R. C.: The other side of droughts: wet extremes and topography
416 as buffers of negative drought effects in an Amazonian forest, *New Phytologist*, 229, 1995-2006,
417 <https://doi.org/10.1111/nph.17005>, 2021.

418 Fan, Y., Miguez-Macho, G., Jobbágy, E. G., Jackson, R. B., and Otero-Casal, C.: Hydrologic regulation of plant rooting depth,
419 *Proceedings of the National Academy of Sciences*, 114, 10572-10577, 10.1073/pnas.1712381114, 2017.

420 Federer, C., Vörösmarty, C., and Fekete, B.: Sensitivity of annual evaporation to soil and root properties in two models of
421 contrasting complexity, *Journal of Hydrometeorology*, 4, 1276-1290, 2003.

422 Feng, W., Zhong, M., Lemoine, J.-M., Biancale, R., Hsu, H.-T., and Xia, J.: Evaluation of groundwater depletion in North
423 China using the Gravity Recovery and Climate Experiment (GRACE) data and ground-based measurements, *Water Resources*
424 *Research*, 49, 2110-2118, <https://doi.org/10.1002/wrcr.20192>, 2013.

425 Gao, H., Hrachowitz, M., Schymanski, S. J., Fenicia, F., Sriwongsitanon, N., and Savenije, H. H. G.: Climate controls how
426 ecosystems size the root zone storage capacity at catchment scale, *Geophysical Research Letters*, 41, 7916-7923,
427 <https://doi.org/10.1002/2014GL061668>, 2014.

428 Gao, H., Hrachowitz, M., Wang-Erlandsson, L., Fenicia, F., Xi, Q., Xia, J., Shao, W., Sun, G., and Savenije, H. H. G.: Root
429 zone in the Earth system, *Hydrol. Earth Syst. Sci.*, 28, 4477-4499, 10.5194/hess-28-4477-2024, 2024.

430 Gebremichael, M., Krajewski, W. F., Morrissey, M., Langerud, D., Huffman, G. J., and Adler, R.: Error Uncertainty Analysis
431 of GPCP Monthly Rainfall Products: A Data-Based Simulation Study, *Journal of Applied Meteorology*, 42, 1837-1848,
432 10.1175/1520-0450(2003)042<1837:Euaogm>2.0.Co;2, 2003.

433 Ghiggi, G., Humphrey, V., Seneviratne, S. I., and Gudmundsson, L.: G-RUN ENSEMBLE: A Multi-Forcing Observation-
434 Based Global Runoff Reanalysis, *Water Resources Research*, 57, e2020WR028787, <https://doi.org/10.1029/2020WR028787>,
435 2021.

436 Giardina, F., Gentile, P., Konings, A. G., Seneviratne, S. I., and Stocker, B. D.: Diagnosing evapotranspiration responses to
437 water deficit across biomes using deep learning, *New Phytologist*, n/a, <https://doi.org/10.1111/nph.19197>, 2023.

438 Gou, J. and Soja, B.: Global high-resolution total water storage anomalies from self-supervised data assimilation using deep
439 learning algorithms, *Nature Water*, 2, 139-150, 10.1038/s44221-024-00194-w, 2024.

440 Goulden, M. L. and Bales, R. C.: California forest die-off linked to multi-year deep soil drying in 2012–2015 drought, *Nature*
441 *Geoscience*, 12, 632-637, 10.1038/s41561-019-0388-5, 2019.

442 Hahm, W. J., Rempe, D., Dralle, D., Dawson, T., and Dietrich, W.: Oak transpiration drawn from the weathered bedrock
443 vadose zone in the summer dry season, *Water Resources Research*, 56, e2020WR027419, 2020.

444 Hahm, W. J., Dralle, D. N., Rempe, D. M., Bryk, A. B., Thompson, S. E., Dawson, T. E., and Dietrich, W. E.: Low Subsurface
445 Water Storage Capacity Relative to Annual Rainfall Decouples Mediterranean Plant Productivity and Water Use From Rainfall
446 Variability, *Geophysical Research Letters*, 46, 6544-6553, <https://doi.org/10.1029/2019GL083294>, 2019.

447 Hain, C. R., Crow, W. T., Anderson, M. C., and Yilmaz, M. T.: Diagnosing Neglected Soil Moisture Source–Sink Processes
448 via a Thermal Infrared–Based Two-Source Energy Balance Model, *Journal of Hydrometeorology*, 16, 1070-1086,
449 <https://doi.org/10.1175/JHM-D-14-0017.1>, 2015.

450 Hersbach, H., Bell, B., Berrisford, P., Hirahara, S., Horányi, A., Muñoz-Sabater, J., Nicolas, J., Peubey, C., Radu, R., Schepers,
451 D., Simmons, A., Soci, C., Abdalla, S., Abellan, X., Balsamo, G., Bechtold, P., Biavati, G., Bidlot, J., Bonavita, M., De Chiara,
452 G., Dahlgren, P., Dee, D., Diamantakis, M., Dragani, R., Flemming, J., Forbes, R., Fuentes, M., Geer, A., Haimberger, L.,
453 Healy, S., Hogan, R. J., Hólm, E., Janisková, M., Keeley, S., Laloyaux, P., Lopez, P., Lupu, C., Radnoti, G., de Rosnay, P.,
454 Rozum, I., Vamborg, F., Villaume, S., and Thépaut, J.-N.: The ERA5 global reanalysis, *Quarterly Journal of the Royal
455 Meteorological Society*, 146, 1999-2049, <https://doi.org/10.1002/qj.3803>, 2020.

456 Hulsman, P., Keune, J., Koppa, A., Schellekens, J., and Miralles, D. G.: Incorporating Plant Access to Groundwater in Existing
457 Global, Satellite-Based Evaporation Estimates, *Water Resources Research*, 59, e2022WR033731,
458 <https://doi.org/10.1029/2022WR033731>, 2023.

459 Humphrey, V., Zscheischler, J., Ciais, P., Gudmundsson, L., Sitch, S., and Seneviratne, S. I.: Sensitivity of atmospheric CO₂
460 growth rate to observed changes in terrestrial water storage, *Nature*, 560, 628-631, 10.1038/s41586-018-0424-4, 2018.

461 Jackson, R. B., Moore, L. A., Hoffmann, W. A., Pockman, W. T., and Linder, C. R.: Ecosystem rooting depth determined with
462 caves and DNA, *Proceedings of the National Academy of Sciences*, 96, 11387-11392, doi:10.1073/pnas.96.20.11387, 1999.

463 Jiménez-Rodríguez, C. D., Sulis, M., and Schymanski, S.: Exploring the role of bedrock representation on plant transpiration
464 response during dry periods at four forested sites in Europe, *Biogeosciences*, 19, 3395-3423, 2022.

465 Koirala, S., Jung, M., Reichstein, M., de Graaf, I. E. M., Camps-Valls, G., Ichii, K., Papale, D., Ráduly, B., Schwalm, C. R.,
466 Tramontana, G., and Carvalhais, N.: Global distribution of groundwater-vegetation spatial covariation, *Geophysical Research
467 Letters*, 44, 4134-4142, <https://doi.org/10.1002/2017GL072885>, 2017.

468 Koppa, A., Rains, D., Hulsman, P., Poyatos, R., and Miralles, D. G.: A deep learning-based hybrid model of global terrestrial
469 evaporation, *Nature Communications*, 13, 1912, 10.1038/s41467-022-29543-7, 2022.

470 Kuzyakov, Y. and Razavi, B. S.: Rhizosphere size and shape: Temporal dynamics and spatial stationarity, *Soil Biology and
471 Biochemistry*, 135, 343-360, <https://doi.org/10.1016/j.soilbio.2019.05.011>, 2019.

472 Li, B., Rodell, M., and Famiglietti, J. S.: Groundwater variability across temporal and spatial scales in the central and
473 northeastern U.S, *Journal of Hydrology*, 525, 769-780, <https://doi.org/10.1016/j.jhydrol.2015.04.033>, 2015.

474 Li, B., Rodell, M., Kumar, S., Beaudoin, H. K., Getirana, A., Zaitchik, B. F., de Goncalves, L. G., Cossetin, C., Bhanja, S.,
475 and Mukherjee, A.: Global GRACE data assimilation for groundwater and drought monitoring: Advances and challenges,
476 *Water Resources Research*, 55, 7564-7586, 2019.

477 Liu, P.-W., Famiglietti, J. S., Purdy, A. J., Adams, K. H., McEvoy, A. L., Reager, J. T., Bindlish, R., Wiese, D. N., David, C.
478 H., and Rodell, M.: Groundwater depletion in California's Central Valley accelerates during megadrought, *Nature*
479 *Communications*, 13, 7825, 10.1038/s41467-022-35582-x, 2022.

480 Livneh, B. and Hoerling, M. P.: The Physics of Drought in the U.S. Central Great Plains, *Journal of Climate*, 29, 6783-6804,
481 <https://doi.org/10.1175/JCLI-D-15-0697.1>, 2016.

482 Mastrotheodoros, T., Pappas, C., Molnar, P., Burlando, P., Manoli, G., Parajka, J., Rigon, R., Szeles, B., Bottazzi, M.,
483 Hadjidoukas, P., and Faticchi, S.: More green and less blue water in the Alps during warmer summers, *Nature Climate Change*,
484 10, 155-161, 10.1038/s41558-019-0676-5, 2020.

485 Maxwell, R. M. and Condon, L. E.: Connections between groundwater flow and transpiration partitioning, *Science*, 353, 377-
486 380, doi:10.1126/science.aaf7891, 2016.

487 McCabe, G. J. and Markstrom, S. L.: A monthly water-balance model driven by a graphical user interface, US Geological
488 Survey Reston, VA, USA2007.

489 McCormick, E. L., Dralle, D. N., Hahm, W. J., Tune, A. K., Schmidt, L. M., Chadwick, K. D., and Rempe, D. M.: Widespread
490 woody plant use of water stored in bedrock, *Nature*, 597, 225-229, 10.1038/s41586-021-03761-3, 2021.

491 McKee, T. B., Doesken, N. J., and Kleist, J.: The relationship of drought frequency and duration to time scales, *Proceedings*
492 *of the 8th Conference on Applied Climatology*, 179-183,

493 Miguez-Macho, G. and Fan, Y.: Spatiotemporal origin of soil water taken up by vegetation, *Nature*, 598, 624-628,
494 10.1038/s41586-021-03958-6, 2021.

495 Miralles, D. G., Bonte, O., Koppa, A., Villanueva, O. B., Tronquo, E., Zhong, F., Beck, H., Hulsman, P., Dorigo, W., and
496 Verhoest, N. E.: GLEAM4: global land evaporation dataset at 0.1 resolution from 1980 to near present, 2024.

497 Miralles, D. G., Jiménez, C., Jung, M., Michel, D., Ershadi, A., McCabe, M. F., Hirschi, M., Martens, B., Dolman, A. J.,
498 Fisher, J. B., Mu, Q., Seneviratne, S. I., Wood, E. F., and Fernández-Prieto, D.: The WACMOS-ET project – Part 2: Evaluation
499 of global terrestrial evaporation data sets, *Hydrol. Earth Syst. Sci.*, 20, 823-842, 10.5194/hess-20-823-2016, 2016.

500 Nash, J. E. and Sutcliffe, J. V.: River flow forecasting through conceptual models part I—A discussion of principles, *Journal*
501 *of hydrology*, 10, 282-290, 1970.

502 Naumburg, E., Mata-gonzalez, R., Hunter, R. G., McLendon, T., and Martin, D. W.: Phreatophytic Vegetation and
503 Groundwater Fluctuations: A Review of Current Research and Application of Ecosystem Response Modeling with an
504 Emphasis on Great Basin Vegetation, *Environmental Management*, 35, 726-740, 10.1007/s00267-004-0194-7, 2005.

505 Novick, K. A., Ficklin, D. L., Baldocchi, D., Davis, K. J., Ghezzehei, T. A., Konings, A. G., MacBean, N., Raoult, N., Scott,
506 R. L., Shi, Y., Sulman, B. N., and Wood, J. D.: Confronting the water potential information gap, *Nature Geoscience*, 15, 158-
507 164, 10.1038/s41561-022-00909-2, 2022.

508 Orellana, F., Verma, P., Loheide II, S. P., and Daly, E.: Monitoring and modeling water-vegetation interactions in groundwater-
509 dependent ecosystems, *Reviews of Geophysics*, 50, <https://doi.org/10.1029/2011RG000383>, 2012.

510 Pérez-Ruiz, E. R., Vivoni, E. R., and Sala, O. E.: Seasonal carryover of water and effects on carbon dynamics in a dryland
511 ecosystem, *Ecosphere*, 13, e4189, 2022.

512 Peterson, T. J., Saft, M., Peel, M. C., and John, A.: Watersheds may not recover from drought, *Science*, 372, 745-749,
513 doi:10.1126/science.abd5085, 2021.

514 Rempe, D. M. and Dietrich, W. E.: Direct observations of rock moisture, a hidden component of the hydrologic cycle,
515 *Proceedings of the National Academy of Sciences*, 115, 2664-2669, doi:10.1073/pnas.1800141115, 2018.

516 Rodell, M., Velicogna, I., and Famiglietti, J. S.: Satellite-based estimates of groundwater depletion in India, *Nature*, 460, 999-
517 1002, 10.1038/nature08238, 2009.

518 Rodell, M., Chao, B. F., Au, A. Y., Kimball, J. S., and McDonald, K. C.: Global biomass variation and its geodynamic effects:
519 1982–98, *Earth Interactions*, 9, 1-19, 2005.

520 Rodell, M., Famiglietti, J. S., Wiese, D. N., Reager, J. T., Beaudoin, H. K., Landerer, F. W., and Lo, M. H.: Emerging trends
521 in global freshwater availability, *Nature*, 557, 651-659, 10.1038/s41586-018-0123-1, 2018.

522 Rohde, M. M., Albano, C. M., Huggins, X., Klausmeyer, K. R., Morton, C., Sharman, A., Zaveri, E., Saito, L., Freed, Z.,
523 Howard, J. K., Job, N., Richter, H., Toderich, K., Rodella, A.-S., Gleeson, T., Huntington, J., Chandanpurkar, H. A., Purdy,
524 A. J., Famiglietti, J. S., Singer, M. B., Roberts, D. A., Caylor, K., and Stella, J. C.: Groundwater-dependent ecosystem map
525 exposes global dryland protection needs, *Nature*, 632, 101-107, 10.1038/s41586-024-07702-8, 2024.

526 Schlemmer, L., Schär, C., Lüthi, D., and Strebel, L.: A Groundwater and Runoff Formulation for Weather and Climate Models,
527 *Journal of Advances in Modeling Earth Systems*, 10, 1809-1832, <https://doi.org/10.1029/2017MS001260>, 2018.

528 Scott, R. L. and Biederman, J. A.: Critical Zone Water Balance Over 13 Years in a Semiarid Savanna, *Water Resources*
529 *Research*, 55, 574-588, <https://doi.org/10.1029/2018WR023477>, 2019.

530 Seneviratne, S. I., Corti, T., Davin, E. L., Hirschi, M., Jaeger, E. B., Lehner, I., Orlowsky, B., and Teuling, A. J.: Investigating
531 soil moisture–climate interactions in a changing climate: A review, *Earth-Science Reviews*, 99, 125-161,
532 <https://doi.org/10.1016/j.earscirev.2010.02.004>, 2010.

533 Speich, M. J., Lischke, H., and Zappa, M.: Testing an optimality-based model of rooting zone water storage capacity in
534 temperate forests, *Hydrology and Earth System Sciences*, 22, 4097-4124, 2018.

535 Stocker, B. D., Tumber-Dávila, S. J., Konings, A. G., Anderson, M. C., Hain, C., and Jackson, R. B.: Global patterns of water
536 storage in the rooting zones of vegetation, *Nature Geoscience*, 10.1038/s41561-023-01125-2, 2023.

537 Stoy, P. C., El-Madany, T. S., Fisher, J. B., Gentine, P., Gerken, T., Good, S. P., Klosterhalfen, A., Liu, S., Miralles, D. G.,
538 and Perez-Priego, O.: Reviews and syntheses: Turning the challenges of partitioning ecosystem evaporation and transpiration
539 into opportunities, *Biogeosciences*, 16, 3747-3775, 2019.

540 Sulla-Menashe, D. and Friedl, M. A.: User guide to collection 6 MODIS land cover (MCD12Q1 and MCD12C1) product,
541 USGS: Reston, VA, USA, 1-18, 2018.

542 Sun, Q., Miao, C., Duan, Q., Ashouri, H., Sorooshian, S., and Hsu, K.-L.: A Review of Global Precipitation Data Sets: Data
543 Sources, Estimation, and Intercomparisons, *Reviews of Geophysics*, 56, 79-107, <https://doi.org/10.1002/2017RG000574>,
544 2018.

545 Teuling, A. J., Seneviratne, S. I., Williams, C., and Troch, P. A.: Observed timescales of evapotranspiration response to soil
546 moisture, *Geophysical Research Letters*, 33, <https://doi.org/10.1029/2006GL028178>, 2006.

547 Thompson, S. E., Harman, C. J., Konings, A. G., Sivapalan, M., Neal, A., and Troch, P. A.: Comparative hydrology across
 548 AmeriFlux sites: The variable roles of climate, vegetation, and groundwater, *Water Resources Research*, 47,
 549 <https://doi.org/10.1029/2010WR009797>, 2011.

550 Ukkola, A. M., De Kauwe, M. G., Roderick, M. L., Burrell, A., Lehmann, P., and Pitman, A. J.: Annual precipitation explains
 551 variability in dryland vegetation greenness globally but not locally, *Glob Chang Biol*, 27, 4367-4380, 10.1111/gcb.15729,
 552 2021.

553 Vereecken, H., Amelung, W., Bauke, S. L., Bogen, H., Brüggemann, N., Montzka, C., Vanderborght, J., Bechtold, M.,
 554 Blöschl, G., Carminati, A., Javaux, M., Konings, A. G., Kusche, J., Neuweiler, I., Or, D., Steele-Dunne, S., Verhoef, A.,
 555 Young, M., and Zhang, Y.: Soil hydrology in the Earth system, *Nature Reviews Earth & Environment*, 3, 573-587,
 556 10.1038/s43017-022-00324-6, 2022.

557 Wang, S., Li, J., and Russell, H. A. J.: Methods for Estimating Surface Water Storage Changes and Their Evaluations, *Journal*
 558 *of Hydrometeorology*, 24, 445-461, <https://doi.org/10.1175/JHM-D-22-0098.1>, 2023a.

559 Wang, T., Wu, Z., Wang, P., Wu, T., Zhang, Y., Yin, J., Yu, J., Wang, H., Guan, X., Xu, H., Yan, D., and Yan, D.: Plant-
 560 groundwater interactions in drylands: A review of current research and future perspectives, *Agricultural and Forest*
 561 *Meteorology*, 341, 109636, <https://doi.org/10.1016/j.agrformet.2023.109636>, 2023b.

562 Wang-Erlandsson, L., Bastiaanssen, W. G. M., Gao, H., Jägermeyr, J., Senay, G. B., van Dijk, A. I. J. M., Guerschman, J. P.,
 563 Keys, P. W., Gordon, L. J., and Savenije, H. H. G.: Global root zone storage capacity from satellite-based evaporation, *Hydrol.*
 564 *Earth Syst. Sci.*, 20, 1459-1481, 10.5194/hess-20-1459-2016, 2016.

565 Watkins, M. M., Wiese, D. N., Yuan, D.-N., Boening, C., and Landerer, F. W.: Improved methods for observing Earth's time
 566 variable mass distribution with GRACE using spherical cap mascons, *Journal of Geophysical Research: Solid Earth*, 120,
 567 2648-2671, <https://doi.org/10.1002/2014JB011547>, 2015.

568 Wieder, W., Boehnert, J., Bonan, G., and Langseth, M.: Regrided Harmonized World Soil Database v1. 2. Data Set. Available
 569 on-Line [[Http://Daac. Ornl. Gov](http://Daac.Ornl.Gov)] from Oak Ridge National Laboratory Distributed Active Archive Center, Oak Ridge,
 570 Tennessee, USA, 2014.

571 Wiese, D. N., Landerer, F. W., and Watkins, M. M.: Quantifying and reducing leakage errors in the JPL RL05M GRACE
 572 mascon solution, *Water Resources Research*, 52, 7490-7502, <https://doi.org/10.1002/2016WR019344>, 2016.

573 Yang, Y., Donohue, R. J., and McVicar, T. R.: Global estimation of effective plant rooting depth: Implications for hydrological
 574 modeling, *Water Resources Research*, 52, 8260-8276, <https://doi.org/10.1002/2016WR019392>, 2016.

575 Zhao, M., A. G., Liu, Y., and Konings, A. G.: Evapotranspiration frequently increases during droughts, *Nature Climate*
 576 *Change*, 12, 1024-1030, 10.1038/s41558-022-01505-3, 2022.

577 Zhao, M., A. G., Zhang, J., Velicogna, I., Liang, C., and Li, Z.: Ecological restoration impact on total terrestrial water storage,
 578 *Nature Sustainability*, 4, 56-62, 10.1038/s41893-020-00600-7, 2021.

579